Monthly Notices
of the
ROYAL ASTRONOMICAL SOCIETY

MNRAS **449,** 2576–2587 (2015) doi:10.1093/mnras/stv490

A new spin on discs of satellite galaxies

Marius Cautun,* Wenting Wang,* Carlos S. Frenk and Till Sawala

Department of Physics, Institute for Computational Cosmology, University of Durham, South Road, Durham DH1 3LE, UK

Accepted 2015 March 3. Received 2015 February 19; in original form 2014 October 28

ABSTRACT

We investigate the angular and kinematic distributions of satellite galaxies around a large sample of bright isolated primaries in the spectroscopic and photometric catalogues of the Sloan Digital Sky Survey (SDSS). We detect significant anisotropy in the spatial distribution of satellites. To test whether this anisotropy could be related to the rotating discs of satellites recently found by Ibata et al. in a sample of SDSS galaxies, we repeat and extend their analysis. Ibata et al. found an excess of satellites on opposite sides of their primaries having anticorrelated radial velocities. We find that this excess is sensitive to small changes in the sample selection criteria which can greatly reduce its significance. In addition, we find no evidence for correspondingly correlated velocities for satellites observed on the same side of their primaries, which would be expected for rotating discs of satellites. We conclude that the detection of rotating planes of satellites in the observational sample of Ibata et al. is not robust to changes in the sample selection criteria. We compare our data to the Λ cold dark matter Millennium simulations populated with galaxies according to the semi-analytic model of Guo et al. We find excellent agreement with the spatial distribution of satellites in the SDSS data and the lack of a strong signal from coherent rotation.

Key words: galaxies: abundances – galaxies: haloes – galaxies: statistics – dark matter.

1 INTRODUCTION

It has been known for decades that the 11 'classical' satellites of the Milky Way (MW) define a thin plane (Lynden-Bell 1976) and that some of the fainter satellites, tidal streams and young globular clusters have an anisotropic distribution reminiscent of this plane (Metz, Kroupa & Jerjen 2009a; Pawlowski, Pflamm-Altenburg & Kroupa 2012a). Many members of this 'disc of satellites' have a common rotation direction and it has been claimed that the plane is a rotationally stabilized structure (Metz, Kroupa & Libeskind 2008; Pawlowski & Kroupa 2013). Similarly, the spatial distribution of satellites around Andromeda is also thought to be anisotropic (Koch & Grebel 2006; McConnachie & Irwin 2006), with 15 out of 27 satellites observed by the Pan-Andromeda Archaeological Survey (PAndAS; McConnachie et al. 2009) located in a very thin plane in which 13 out of the 15 satellites share the same sense of rotation (Ibata et al. 2013).

Anisotropies in the distribution of satellites are a clear prediction of the Λ cold dark matter (ΛCDM) paradigm (Libeskind et al. 2005, 2009, 2011; Zentner et al. 2005; Deason et al. 2011; Wang, Frenk & Cooper 2013). Such flattened satellite distributions, dubbed 'great pancakes', can arise from the infall of satellites along the spine of filaments (Libeskind et al. 2005), which in turn determine the preferential points at which satellites enter the virial radius of the host halo (Libeskind et al. 2011, 2014). Correlated accretion along filaments has also been ascribed by Deason et al. (2011) as the cause of the satellite anisotropies observed in the 'GIMIC' gasdynamic simulation (Crain et al. 2009); they found a polar alignment of satellite discs (with more than 10 bright members) for 20 per cent of the cases. The flattening effects of anisotropic accretion are greatly enhanced in the case when subhaloes are accreted in groups (Li & Helmi 2008; though Metz et al. 2009b claimed that this would not explain the MW satellite plane), although such occurrences are rare for bright satellites and only become more frequent for less massive subhaloes (Wang et al. 2013). The imprint of anisotropic accretion is retained in the dynamics of satellites, with a significant population of subhaloes corotating with the spin of the host halo (Libeskind et al. 2009; Lovell et al. 2011, for galactic haloes; Shaw et al. 2006; Warnick & Knebe 2006 for cluster mass haloes). An alternative view that has been put forward is that the satellites do not reside in dark matter substructures, but instead are formed from tidal debris produced during galaxy-galaxy interactions, which could also result in the formation of satellite planes (e.g. Fouquet et al. 2012; Hammer et al. 2013; Yang et al. 2014).

Although flattened satellite distributions are common in ΛCDM, the degree of flattening of the MW and Andromeda satellites is atypical. Wang et al. (2013) found that 5–10 per cent of satellite systems are as flat as the MW's 11 classical satellites but, when the requirement that the velocities of at least eight of the 11 satellites should point within the narrow angle claimed by Pawlowski & Kroupa

* E-mail: m.c.cautun@durham.ac.uk (MC); wenting.wang@durham.ac.uk (WW)

(2013) for the MW satellites, this fraction decreases to ∼1 per cent. Pawlowski et al. (2012b) claimed that there is only a 0.5 per cent chance that this alignment is due to filamentary satellite accretion. In the case of Andromeda's thin satellite plane, Bahl & Baumgardt (2014, but see Pawlowski et al. 2014) found that, while similar spatial distributions of satellites are quite common in ΛCDM, there is only a 2 per cent chance that 13 out of the 15 members in the plane share the same sense of rotation. In a similar study, Ibata et al. (2014c) found an even lower occurrence rate for Andromeda's thin plane in ΛCDM simulations.

The presence of such highly flattened satellite systems in the Local Group (LG) raises an important question: are such systems ubiquitous around other galaxies, or are they a consequence of the large-scale environment in which the LG is located? While being a member of a pair rather than an isolated halo seems to make little difference for the distribution of satellites (Pawlowski & McGaugh 2014), the effect of the megaparsec-scale environment is still unknown. The crucial role of large-scale modes in determining the properties of the LG was illustrated by Forero-Romero et al. (2011) who, using constrained simulations of the local cosmological volume, found that LG-analogues have highly atypical formation times, assembly histories and times since last major merger when compared to a sample of similar mass halo pairs.

Studies of large samples of galaxies are limited to investigating anisotropies in the satellite distribution with respect to preferential axes defined by the projected galaxy light. For example, late-type galaxies have satellite distributions that are close to isotropic, while the satellites of early-type galaxies are aligned with the major axis of the galaxy's light (Brainerd 2005; Yang et al. 2006; Bailin et al. 2008; Agustsson & Brainerd 2010; Guo et al. 2012; Nierenberg et al. 2012). Such studies have limited power to constrain the full flattening of the satellite distribution when such anisotropies are uncorrelated, or only weakly correlated, with the light distribution of the central host.

Recently, Ibata et al. (2014a, hereafter Ibata14) analysed correlations in the velocities of satellite galaxies observed on opposite sides of their central host. For a sample selected from Sloan Digital Sky Survey (SDSS; Abazajian et al. 2009), they found the most significant effect for an opening angle of $<8^\circ$, for which 20 out of 22 satellite pairs have anticorrelated velocities, suggestive of a rotating disc that contains ∼50 per cent of the satellite population. Ibata et al. (2014a) reported a significance of 4σ for a null hypothesis of an isotropic satellite distribution. They found no such effect in the Millennium II ΛCDM simulations.

In this study, we compare the angular distribution of satellites around external galaxies with the predictions of the Guo et al. (2011) semi-analytic model of galaxy formation model implemented in the Millennium (MS; Springel et al. 2005) and Millennium II (MS-II; Boylan-Kolchin et al. 2009) simulations. We make use of both spectroscopic and photometric SDSS data, limiting our analysis to systems of isolated galaxies with at least one spectroscopic satellite. We use the axis connecting the position of the brightest spectroscopic satellite to its host galaxy to measure the angles at which other satellites appear on the sky. The distribution of this angle is sensitive to anisotropies in the spatial distribution of satellites, as we show using a simple disc model. We compare the resulting angular distribution of satellites with ΛCDM predictions for different central host luminosities and find very good agreement between the two. We also show that the excess of satellite pairs with anticorrelated velocities found by Ibata14 is not robust to changes in sample selection and conclude that the known kinematics of satellites are not in disagreement with ΛCDM predictions.

This paper is organized as follows: Section 2 introduces the observational and simulation data, as well as the selection criteria used to identify isolated galaxies and their satellites; in Section 3, we obtain the angular distribution of SDSS satellites and compare the results with ΛCDM predictions; Section 4 is devoted to studying kinematical signatures of satellite discs and on revisiting the excess of satellite pairs with anticorrelated velocities; we conclude with a short discussion and summary in Section 6.

2 DATA AND SAMPLE SELECTION

We identify isolated galaxies and count their satellites using the methods described by Wang & White (2012, hereafter WW12; see also Wang et al. 2014). We now briefly introduce these methods and describe the data sets that we used.

2.1 SDSS isolated galaxy sample

We select isolated primary galaxies from the New York University Value Added Galaxy Catalogue (NYU-VAGC) 1 (Blanton et al. 2005), which is based on the Seventh Data Release of the SDSS (SDSS/DR7; Abazajian et al. 2009). We require that these galaxies should be brighter than any companion lying within a projected radius of $r_p = 0.5$ Mpc and having line-of-sight velocity difference $c|\Delta z| < 1500\,\mathrm{km\,s^{-1}}$. In order to match the selection criteria used by Ibata14, the results presented in Section 4 use only this sample of isolated primaries.

For the analysis in Section 3, we apply a further isolation selection criterion that takes into account the fact that the SDSS spectroscopic sample is incomplete due to fibre–fibre collisions. To prevent primaries being falsely identified as isolated because of incompleteness in the spectroscopic catalogue, we search for further companions using the photometric SDSS catalogue. We reject primary candidates if they have a photometric companion which is not in the spectroscopic catalogue but satisfies the position and magnitude cuts given above and the probability that its redshift is equal to or less than the primary is larger than 10 per cent. For this last step, we use the photometric redshift distributions from Cunha et al. (2009).

2.2 SDSS satellite galaxy sample

For the analysis described in Section 3, we first split the isolated galaxy sample into three subsamples according to their absolute r-band magnitudes. We use three bins centred on $M_r = -23$, -22 and -21, each of width $\Delta M_r = 1$, as shown in Table 1. We count as satellites all galaxies within a projected radius in the range 20 kpc to

Table 1. The number of isolated galaxies with at least one associated spectroscopic satellite. The MS and MS-II data correspond to the average number of isolated galaxies per line of sight, because multiple lines of sight were used to construct the mock data.

host M_r range	SDSS	MS	MS-II
$-22.5 \geq M_r \geq -23.5$	4211	16 430	111
$-21.5 \geq M_r \geq -22.5$	16 532	112 100	938
$-20.5 \geq M_r \geq -21.5$	8519	235 360	2010

the virial radius, $R_{\rm v}$, with $R_{\rm v} = 500$, 315 and 150 kpc, which correspond to the median virial radii of haloes hosting the galaxies found in each of our luminosity bins.[1] Out of all the isolated primaries, we keep only those which have at least one spectroscopic satellite within a projected distance between 20 kpc and $R_{\rm v}$ and having a line-of-sight velocity difference, $c|\Delta z| < 300\,{\rm km\,s^{-1}}$. The number of isolated galaxies satisfying these criteria is given in Table 1.

We are only interested in isolated primaries with spectroscopically associated satellites since we want to determine a preferential axis that can be used to probe anisotropies in the satellite distribution. The relative position of the satellite with respect to its host represents such a reference axis, $\boldsymbol{x}_{\rm BS}$, since the satellite is more likely to be found along the direction where there is an excess of satellites. If an isolated galaxy has two or more spectroscopic satellites associated with it, we choose the brightest one because the brightest satellites show the largest degree of anisotropy (Wang et al. 2013; Libeskind et al. 2014).

To compute the angular distribution of satellites, we use the SDSS/DR8 photometric catalogue (Aihara et al. 2011), which we correct statistically for background contamination using the method carefully developed and tested by WW12 (where further details may be found). For each isolated galaxy, we identify objects brighter than apparent magnitude $r = 21$ that are within a projected distance between 20 kpc and $R_{\rm v}$. We then use the redshift of the primary to convert apparent magnitudes into rest-frame r and g magnitudes. Of all potential satellites, we only keep those that have rest-frame colours $g - r \leq 1$, since redder objects are too red to be at the redshift of the primary galaxy[2] (Lares, Lambas & Domínguez 2011; WW12). It is useful to exclude such red galaxies since they add noise without adding signal. This colour cut represents a conservative and safe selection, equivalent to a crude cut in photometric redshift.

For each of these potential satellites, we calculate the angle, $\theta_{\rm BS\cdot S}$, with respect to the reference axis, $\boldsymbol{x}_{\rm BS}$, of the system. We then count the number of satellites as a function of the angle $\theta_{\rm BS\cdot S}$. This count excludes the brightest satellite, for which $\theta_{\rm BS\cdot S} = 0^\circ$ by definition. The background galaxy count is given by the number of objects brighter than $r = 21$ having rest-frame colour $g - r \leq 1$, as evaluated at the redshift of the primary. We estimate this background from the survey as a whole. For each bin in $\theta_{\rm BS\cdot S}$, we subtract the average number of background galaxies expected in this area of the sky. The background fraction for the three primary samples, from brightest to faintest, is 57 per cent, 80 per cent and 94 per cent. The excess counts with respect to a homogeneous galaxy background are assumed to be satellites physically associated with the primary galaxy. Finally, results for different primaries are averaged after making completeness, volume and edge corrections, as described in WW12. The measurement uncertainties are estimated using 100 bootstrap samples over the primary galaxies.

The selection of satellites in the sample used in Section 4 is restricted to galaxies with spectroscopic redshifts following the criteria described in Ibata14. For each isolated primary, we identify galaxies that are at least $\Delta M_{\rm r}^{\rm Sat-Cen} = 1$ mag. fainter than the primary and lie within a projected distance between 20 kpc and $R_{\rm max} = 150$ kpc. We further require that the line-of-sight velocity difference of the satellite be $35\,{\rm km\,s^{-1}} \leq {\rm c}|\Delta {\rm z}| \leq {\rm V}_0 \exp\left(-({\rm R}/300\,{\rm kpc})^{0.8}\right)$, where $V_0 = 300\,{\rm km\,s^{-1}}$ and R is the projected distance from the primary of the satellite candidate. We also limit the analysis to primary galaxies in the redshift range 0.002 to $z_{\rm max} = 0.05$. The final sample consists of all primaries with two or more satellites satisfying the above selection criteria. To assess the robustness of the results we vary each of the selection criteria in turn.

2.3 Mock ΛCDM galaxy catalogue

To construct mock catalogues, we use the semi-analytic galaxy formation model of Guo et al. (2011) implemented in the MS (Springel et al. 2005) and MS-II (Boylan-Kolchin et al. 2009). The semi-analytic model has been calibrated to reproduce the stellar mass, luminosity and autocorrelation functions of low redshift galaxies as inferred from SDSS. The abundance and radial distribution of satellites predicted by the model is in very good agreement with SDSS data (WW12; Wang et al. 2014). The two simulations, the high resolution MS-II and the lower resolution but larger volume MS, complement each other well for the purposes of this study. The Guo et al. (2011) data are publicly available at http://www.mpa-garching.mpg.de/millennium.

We create the simulated catalogues by projecting galaxies along random sightlines and assigning a redshift according to their line-of-sight distance and peculiar velocity. We add a Gaussian random velocity error of $\sigma = 15\,{\rm km\,s^{-1}}$ to the radial velocity to simulate the typical SDSS spectroscopic redshift error. We then apply the same host isolation and satellite identification criteria as in our SDSS data to obtain a mock sample of isolated primaries and their satellites. In Section 4, we use only satellites brighter than an absolute magnitude of $M_{\rm r} = -17$.

To mimic the background in the real data, we only consider as background galaxies those with apparent magnitude $r \leq 21$. The background depth is restricted to the size of the simulation cube, $100\,h^{-1}$ Mpc for MS-II and $500\,h^{-1}$ Mpc for MS. Appendix A4 in WW12 presents extensive tests of the background estimation in mocks like ours, and explicitly compares the background of a projected simulation cube with that of a full light-cone mock. WW12 found that the only difference between the two is the size of the uncertainties, which are larger for the light-cone mocks. This reflects the smaller effective volume of light-cone mocks in the redshift range of interest compared to the effective volume of projected simulation cubes.

In Section 3, we find the angular distribution of satellites by counting all the satellites brighter than $r = 21$ lying within projected distance between 20 kpc and $R_{\rm v}$, from which we subtract the average galaxy background of the mock catalogue. When stacking the counts in each primary magnitude bin, we assign weights to the primaries so as to obtain the same redshift distributions in our mock and SDSS samples. We obtain the same average number of satellites per primary for both mock and real data. We create multiple mock catalogues using 1000 and 25 random sightlines from the MS-II and MS, respectively.

3 SPATIAL DISTRIBUTION OF SATELLITES

In this section, we characterize the anisotropies of the satellite distribution around a large number of primary galaxies. For each system, we define a reference axis, $\boldsymbol{x}_{\rm BS}$, given by the relative position of the

[1] We used the Guo et al. (2011) MS catalogue to find the median virial radii of galaxies in each magnitude range. The virial radius of the brightest bin is larger than 500 kpc but we adopted this value since it corresponds to the projected radius used to identify isolated primaries.

[2] For brevity, we only give here a simplified description of the $g - r$ colour cut. The exact cut applied is stellar mass dependent and includes an elaborate procedure of estimating stellar masses using photometric data. The full procedure is described in WW12.

brightest satellite with respect to the primary galaxy, as described in Section 2.2. This reference axis points towards the direction where an excess of satellites is expected on average, if such an excess exists. We first test this approach using a simplified disc model, and then we apply the method to both observations and mock catalogues.

3.1 A simplified disc model

To illustrate our approach, we use the MS data to construct a simple model where a fraction, $f_{\rm disc}$, of the satellites is distributed on a disc of 30 kpc thickness while the remaining satellites are distributed isotropically. We first identify the 'friends-of-friends' (FOF) group to which each primary galaxy belongs. Members of the FOF group other than the primary are then randomly assigned to be part of the disc or of the isotropic population, depending on the value of $f_{\rm disc}$. Finally, the satellites are spatially rearranged into the disc and isotropic populations such that they have the same radial distribution with respect to the primary as in the undisturbed case.

We create new mock catalogues using these disc models, which we analyse in the same way as the SDSS data. The resulting angular distribution function of satellites is shown in the top panel of Fig. 1, where the y-scale is chosen such that a uniform distribution would correspond to a value of 1. Comparing models with different disc fractions, it is clear that the distribution of angles is sensitive to anisotropy in the satellite spatial distribution. The first striking result is the asymmetry between the $\theta_{\rm BS\cdot S} = 0^\circ$ and $\theta_{\rm BS\cdot S} = 180^\circ$ points, which is unexpected given that, by construction, the satellite distributions have cylindrical symmetry. The asymmetry is due to clustering around interloper galaxies, which although not part of the same FOF group as the primary, are close enough in redshift ($c|\Delta z| < 300\,{\rm km\,s^{-1}}$) to be identified as satellites according to our selection criteria. To quantify this effect, we repeat the analysis requiring that the brightest satellite of each primary (which defines the reference axis) be part of the same FOF group. The result is displayed in the bottom panel of Fig. 1 and shows that the curves in this case are symmetric around $\theta_{\rm BS\cdot S} = 90^\circ$.

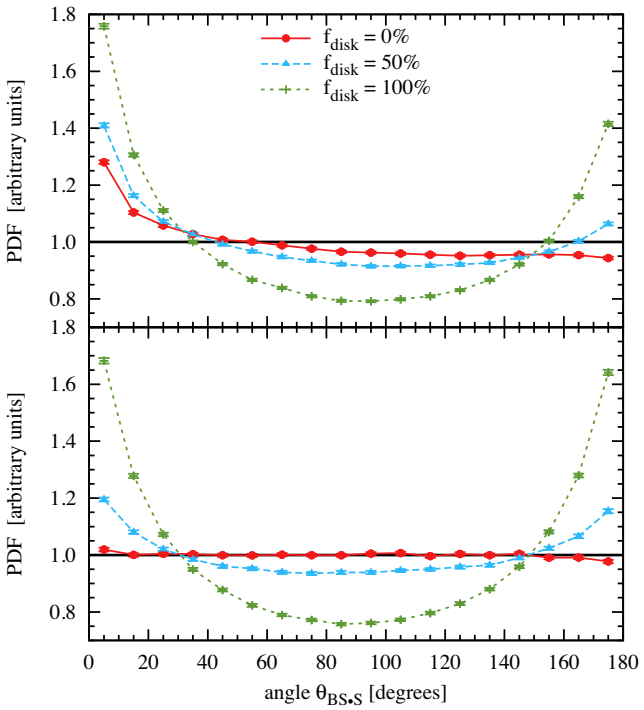

Figure 1. Top panel: the PDF of the angle, $\theta_{\rm BS\cdot S}$, of satellites with respect to the line joining the primary to the brightest satellite in our simplified disc models. In these models a fraction of satellites, $f_{\rm disc}$, of 0 per cent, 50 per cent and 100 per cent are randomly assigned to discs, and the remaining are isotropically distributed around the primary galaxy. Bottom panel: as above, but only for the case where the brightest satellite is part of the same FOF group as the central galaxy.

In addition to clustering around interloper galaxies, there is also clustering around the brightest satellite within an FOF group. This latter effect is not captured in our simplified model where the azimuthal angles are randomized, hence the symmetric curve in the bottom panel of Fig. 1. In the real case, we expect this additional clustering around the brightest satellites to enhance further the asymmetry of the angular distribution of satellites above that seen in the top panel of Fig. 1.

The effect of clustering around the brightest satellite is particularly evident for $\theta_{\rm BS\cdot S} < 90^\circ$, which suggests that we should use the $\theta_{\rm BS\cdot S} > 90^\circ$ part of the curve for quantifying anisotropy. For example, the disc model with $f_{\rm disc} = 0$ per cent shows a nearly flat curve for $\theta_{\rm BS\cdot S} > 90^\circ$, as expected for an isotropic distribution. In contrast, the model with $f_{\rm disc} = 50$ per cent shows 16 per cent more satellites at $\theta_{\rm BS\cdot S} = 180^\circ$ than at $\theta_{\rm BS\cdot S} = 90^\circ$. The difference between the values for the two angles increases to 86 per cent for $f_{\rm disc} = 100$ per cent. This suggests that, with good statistics, i.e. a large enough sample of primaries with at least one spectroscopic satellite, the method can easily quantify the average spatial anisotropy of the satellite distribution. Compared to previous studies (discussed in Section 1), our analysis has the advantage that it is independent of the correlation between the light distribution of the primary galaxy and the anisotropy of the satellite distribution.

3.2 The angular distribution of satellites in the SDSS and mock catalogues

The angular distribution of satellites in the SDSS is given in Fig. 2, with each panel showing the results for a different range of primary magnitudes. We use bootstrap resampling to estimate independently errors for both observational and mock data. For the latter, this accounts for the fact that the same object can be seen multiple times along different sightlines. With the exception of the faintest primary sample, where the errors are comparable to the signal, the data clearly exhibits the telltale sign of an anisotropic distribution: more objects at $\theta_{\rm BS\cdot S} = 180^\circ$ than at $\theta_{\rm BS\cdot S} = 90^\circ$.

Considering first the results from the mock catalogues, it is reassuring that the MS and MS-II, which differ in mass resolution by a factor of 125, give consistent data. This suggests that our results are unaffected by resolution effects or by the treatment of orphan galaxies (i.e. satellites whose dark matter haloes have been stripped). The only notable, although small, difference between the two simulations is in the faintest magnitude bin where most of the signal is due to satellites with $M_{\rm r} \gtrsim -16$ which are not properly resolved in the MS. We have also tested the effect of excluding orphan galaxies from the analysis and find that, in the case of the MS-II, the results hardly change.

In general, we find good agreement between the data and the model predictions. The largest deviations are seen in the central panel of Fig. 2 and are likely caused by the correlated deviations among the data points. The area under each probability distribution function (PDF) is the same, so an excess at one angle leads to a deficit at another. In addition, current semi-analytic models are not able to provide a particularly accurate match to the observed radial and colour distributions of satellites (e.g. Wang et al. 2014). Thus,

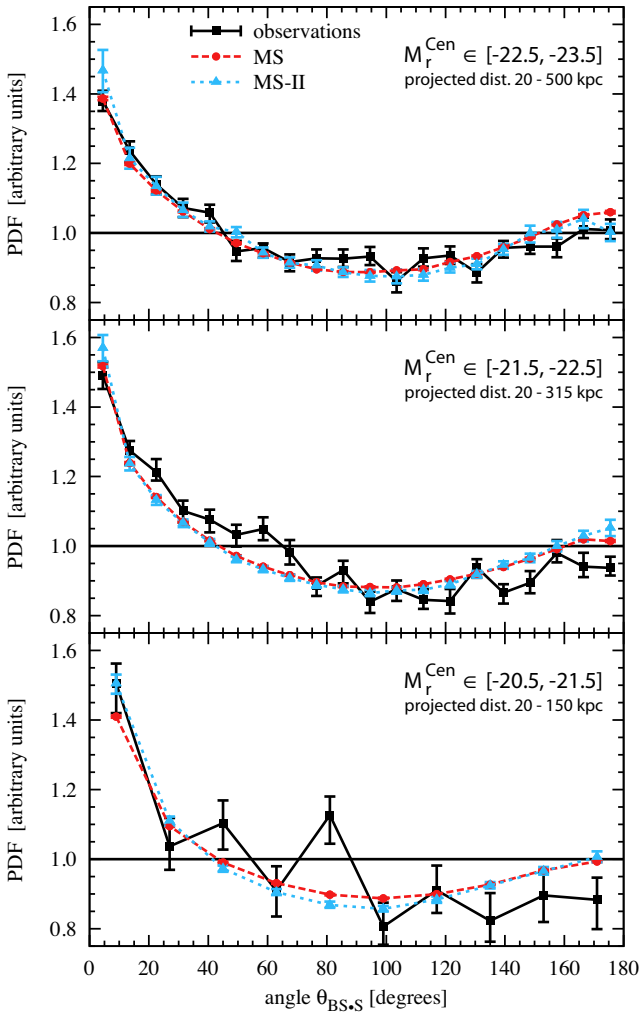

Figure 2. The PDF of the angle, $\theta_{BS\cdot S}$, of satellites with respect to the line joining the primary to the brightest satellite. Results are shown for primaries in three magnitude ranges: $-22.5 \geq M_r^{Cen} \geq -23.5$ (top), $-21.5 \geq M_r^{Cen} \geq -22.5$ (centre) and $-20.5 \geq M_r^{Cen} \geq -21.5$ (bottom). The solid black curve is for the observational data, while the red and blue curves are for the MS and MS-II, respectively.

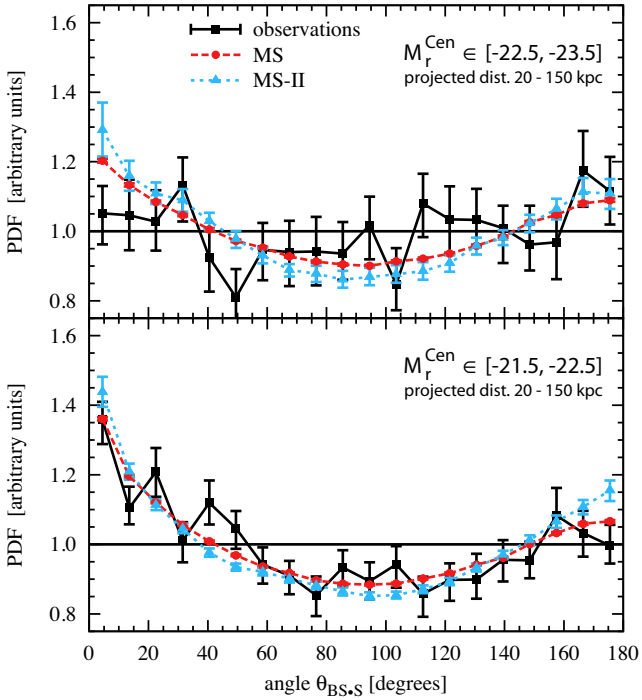

Figure 3. Same as Fig. 2 but restricted to satellites within a projected radial distance of 20 to 150 kpc.

the small differences between data and mocks seen in Fig. 2 may be indicative of inadequacies in the semi-analytic models rather than in ΛCDM itself and are not a concern for the current study.

In Fig. 3, we investigate the spatial anisotropy of satellites in the projected radial range 20–150 kpc, in which Ibata14 claim that ∼50 per cent of satellites form rotating discs. We find again good agreement in the spatial distribution of satellites between data and mocks. In addition, the two mocks, from MS and MS-II, show a reasonable correspondence, although not as good as in Fig. 2. This is very likely due to the treatment of orphan galaxies which, so close to the primary, account for most of the MS satellites (e.g. see Wang et al. 2014).

The main conclusion from Figs 2 and 3 is that the SDSS data agree well with the results from mocks based on a semi-analytic model of galaxy formation in ΛCDM. This is in contrast with recent claims of a conflict between the observed spatial anisotropy in the satellite distribution and the ΛCDM model (e.g. Kroupa 2012). At least according to the test we have performed here, there is no such conflict. In fact, as emphasized amongst others by Libeskind et al. (2005) and Wang et al. (2013), spatial anisotropies are actually *expected* in ΛCDM.

The simulations predict 20 per cent more satellites at $\theta_{BS\cdot S} = 180^\circ$ than at $\theta_{BS\cdot S} = 90^\circ$ for the two brightest bins, and 17 per cent more for the faintest primary sample. If we were to interpret these results in the light of the simplified disc model introduced in Fig. 1, this would suggest that, on average, around ∼50 per cent of the satellites are in a relatively thin plane. Other studies based on cosmological simulations (eg. Libeskind et al. 2005; Wang et al. 2013) showed that planes of satellites exist and, thus, it is natural to expect that the signal seen in Fig. 2 is related to that phenomenon. In cosmological simulations, these planar structures arise from the anisotropic infall of satellite galaxies along filaments, which leads to the formation of flattened, pancake-like satellite distributions (Libeskind et al. 2005).

4 THE ROTATION OF PLANAR STRUCTURES

The motion of satellites around their primary galaxy, as predicted by ΛCDM, is not random, but retains a signature of their anisotropic infall (Lovell et al. 2011). This is illustrated in Fig. 4, where we show the PDF of $\cos\theta_{H\cdot S}$, the cosine of the angle between the halo spin and the orbital momentum of the satellites. These results were obtained by analysing the MS-II real space data for central galaxies in the magnitude range $-20 \geq M_r^{Cen} \geq -23$. They demonstrate that satellite galaxies rotate preferentially in the same direction as their host halo, corroborating the results of Lovell et al. (2011), who analysed the six MW mass haloes of the Aquarius project (Springel et al. 2008). The correlation is strongest for the brightest satellite galaxies. For this sample, the same sense of rotation is shared, on average, by three times more satellites than expected from a random distribution. The figures indicates that ∼15 per cent of the satellites share the same direction of rotation to within 25°, i.e. $\cos\theta_{H\cdot S} \geq 0.9$. While this represents a significant fraction of the population, it falls shorts of the ∼50 per cent fraction found in the SDSS by Ibata14.

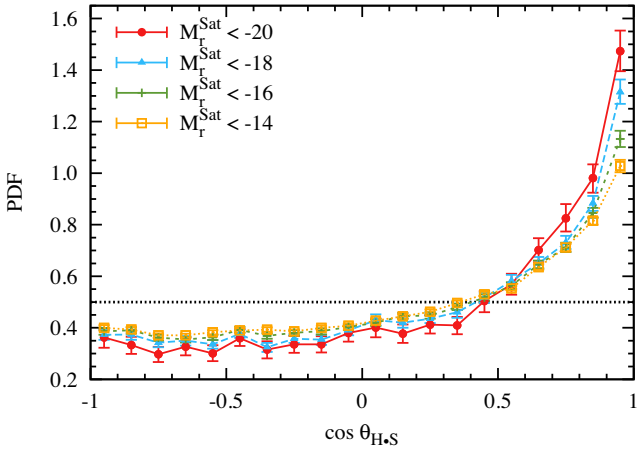

Figure 4. The probability distribution in the MS-II simulation of $\cos\theta_{\mathrm{H\cdot S}}$, the cosine of the angle between the host halo spin and the orbital momentum of its satellites. The black horizontal line corresponds to a uniform distribution.

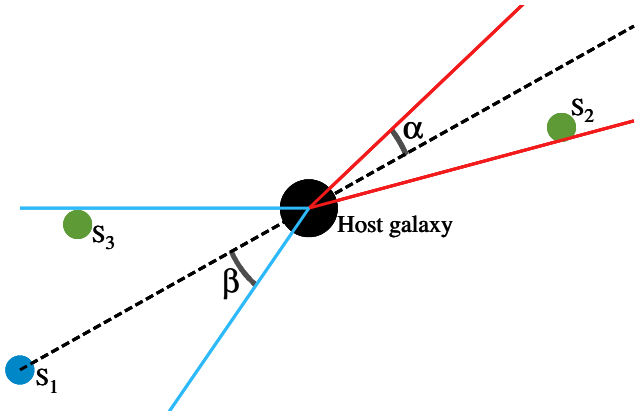

Figure 5. Definition of the tolerance angles, α and β, used to characterize satellite pairs on opposite sides (S_1S_2) and on the same side (S_1S_3) of the primary galaxy, respectively.

To investigate the reported discrepancy between observations and ΛCDM predictions, we have reanalysed the SDSS data used by Ibata14 and extended this kind of analysis in order to obtain better statistics. We are interested in the number of satellite pairs with correlated and anticorrelated line-of-sight velocities as a function of a tolerance angle that characterizes the angular separation of the pair, as illustrated in Fig. 5. The tolerance angle, α, refers to satellite pairs on diametrically opposite sides of the primary, following the same convention as Ibata14, while the tolerance angle, β, refers to pairs on the same side of the host.

4.1 Diametrically opposed satellite pairs

To begin with our analysis follows the exact sample selection criteria described by Ibata14 (see Section 2 for details). At a tolerance angle, $\alpha = 8^\circ$, we were able to recover only 20 pairs of diametrically opposite satellites compared to the 22 pairs reported by Ibata14. This discrepancy is likely due to the use of different versions of

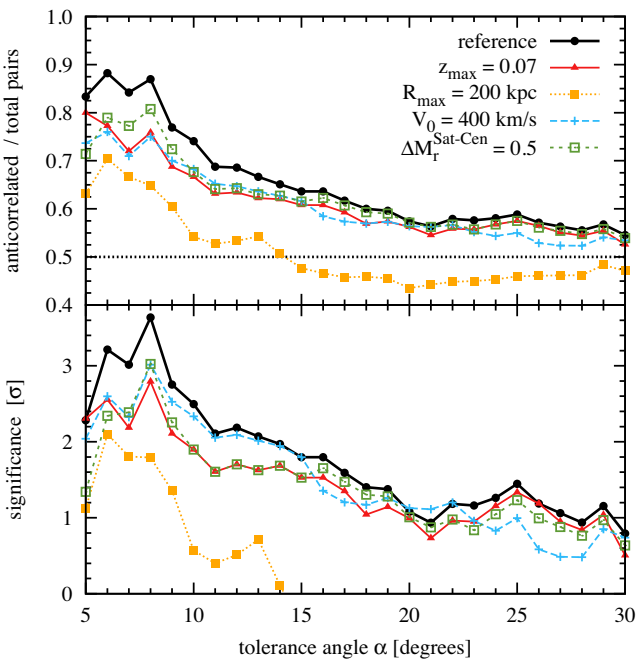

Figure 6. Top panel: the excess of satellite pairs with anticorrelated velocities as a function of the tolerance angle, α, for diametrically opposite pairs. The colour curves show differences from the reference result (solid black) when varying the sample selection criteria, one at a time. Following Ibata14, the reference result assumes $z_{\mathrm{max}} = 0.05$, $R_{\mathrm{max}} = 150\,\mathrm{kpc}$, $V_0 = 300\,\mathrm{km\,s^{-1}}$ and $\Delta M_r^{\mathrm{Sat-Cen}} = 1$. Bottom panel: the significance of the excess of satellite pairs with anticorrelated velocities compared to the null hypothesis of equal numbers of pairs with correlated and anticorrelated velocities.

the NYU-VAGC catalogue.[3] Our original sample missed two pairs with anticorrelated velocities that appear in the sample of Ibata14, corresponding to rows 1 and 18 in their table 1. Using VizieR, we found the satellite pair in row 18 in another catalogue, but we could not identify one of the satellites of the pair in row 1. Nevertheless, we have chosen to include both these pairs in our sample. We also found an additional pair with $\alpha < 8^\circ$, which has correlated velocities, that does not appear in the Ibata14 sample.

The excess of pairs with anticorrelated velocities and its significance as a function of the tolerance angle, α, is shown by the thick black line in Fig. 6. The significance of the excess is evaluated as the sigma-value corresponding to the probability of obtaining such an excess for a binomial distribution of mean 0.5. The inclusion of an additional pair with correlated velocities in our sample results in a smaller excess of anticorrelated pairs than found by Ibata14 and a correspondingly lower statistical significance. The most significant excess is found at $\alpha = 8^\circ$ and corresponds to a 3.6σ significance, compared to a maximum significance of 4σ reported by Ibata14 at the same tolerance angle.

Fig. 6 also shows how the excess of anticorrelated velocity pairs changes when the sample selection criteria are relaxed. We vary one parameter of the selection criteria at a time, keeping the remaining

[3] There is an ambiguity regarding the catalogue used by Ibata14 since the NYU-VAGC website they referenced contains a multitude of catalogues. After trying several of them, we settled on the one which gives absolute magnitudes closest to the values given in table 1 of Ibata14. Nevertheless, there is a ∼0.03 scatter between the absolute magnitudes in our catalogue and those quoted by Ibata14.

parameters at their reference values as given in Section 2. In all cases, we find that the excess of anticorrelated pairs decreases as does the corresponding maximum significance of the excess.

We explore further the sensitivity of the excess of anticorrelated velocity pairs by systematically varying, one at a time, some of the parameters used to select the sample. In each case, we determine the maximum significance of the signal over the range of tolerance angles, $5^\circ \leq \alpha \leq 30^\circ$. With few exceptions, the maximum significance is found for $\alpha = 8^\circ$. The maximum significance as function of some of the main parameters in the selection criteria is plotted in Fig. 7. For clarity, the reference values for each parameter are shown as a vertical grey line. We find that small variations in the sample selection parameters can lead to a significant reduction in the significance of the observed excess of anticorrelated velocity pairs. Except for a few values, the maximum significance is below the 3σ level.

In Table 2, we list the total number of pairs and the number of pairs with anticorrelated velocities for the samples plotted in Fig. 7. If we tighten the selection criteria, the signature of rotating satellite systems is still present, though in most cases its significance is reduced, since the resulting sample is a subset of the reference sample. Relaxing the $z_{\rm max}$ or the $\Delta M_r^{\rm Sat-Cen}$ selection criteria adds at most a small number of new pairs. Increasing $z_{\rm max}$ from 0.05 to 0.1 adds eight extra pairs, while decreasing $\Delta M_r^{\rm Sat-Cen}$ from 1 mag to 0 mag adds six additional pairs. So, for these cases, the measurement is always dominated by the 23 pairs found in the reference sample. In contrast, relaxing $R_{\rm max}$ and $V_{\rm max}$ adds significantly more pairs. Increasing $R_{\rm max}$ from 150 to 300 kpc adds 57 new pairs. Out of these, only 28, exactly half the sample, have anticorrelated velocities. Similarly, increasing $V_{\rm max}$ from 300 to 500 km s^{-1} adds 29 new pairs, with 14 of them, again half the sample, having anticorrelated velocities. Thus, there is no signature of a rotating disc for $V_{\rm max} \geq 300\,{\rm km\,s^{-1}}$ or for $R_{\rm max} \geq 150$ kpc. Any large excess of pairs with anticorrelated velocities seen in Fig. 7 is therefore entirely driven by the reference sample, since the measurements are not independent: they all contain most or all of the 23 pairs of the default sample.

The choices made by Ibata14 reflect various compromises (R. Ibata, private communication). The maximum redshift cut, $z_{\rm max} = 0.05$, was chosen because this value has been commonly used in similar studies to avoid including very bright satellites. The search radius, $R_{\rm max} = 150$ kpc, was chosen to match the M31 PAnDAS survey, while the velocity threshold, $V_{\rm max} = 300\,{\rm km\,s^{-1}}$, corresponds to twice the central velocity dispersion of Andromeda. The maximum magnitude difference, $\Delta M_r^{\rm Sat-Cen} = 1$, between satellites and the central galaxy was chosen in order to discard objects that are too close in brightness to the host.

These choices, of course, are to some extent arbitrary. For example, increasing the maximum redshift range from $z_{\rm max} = 0.05$ to 0.07 adds mainly bright primaries with absolute r-band magnitudes in the range $[-22.6, -22.0]$ which already includes more than half of the primaries in the reference sample. Similarly, increasing the maximum radius used to identify satellites from $R_{\rm max} = 150$ to 200 kpc is not unreasonable given that most of the galaxies in our sample occupy haloes with a virial radius larger than 200 kpc. The sensitivity of the results to the details of the sample selection lead us to conclude that the detection of systemic rotation in the satellite population with current observational samples is not robust.

4.2 Same-side satellite pairs

If the excess of pairs with *anticorrelated* velocities on opposite sides of the host were attributable to rotating discs of satellites, an equal

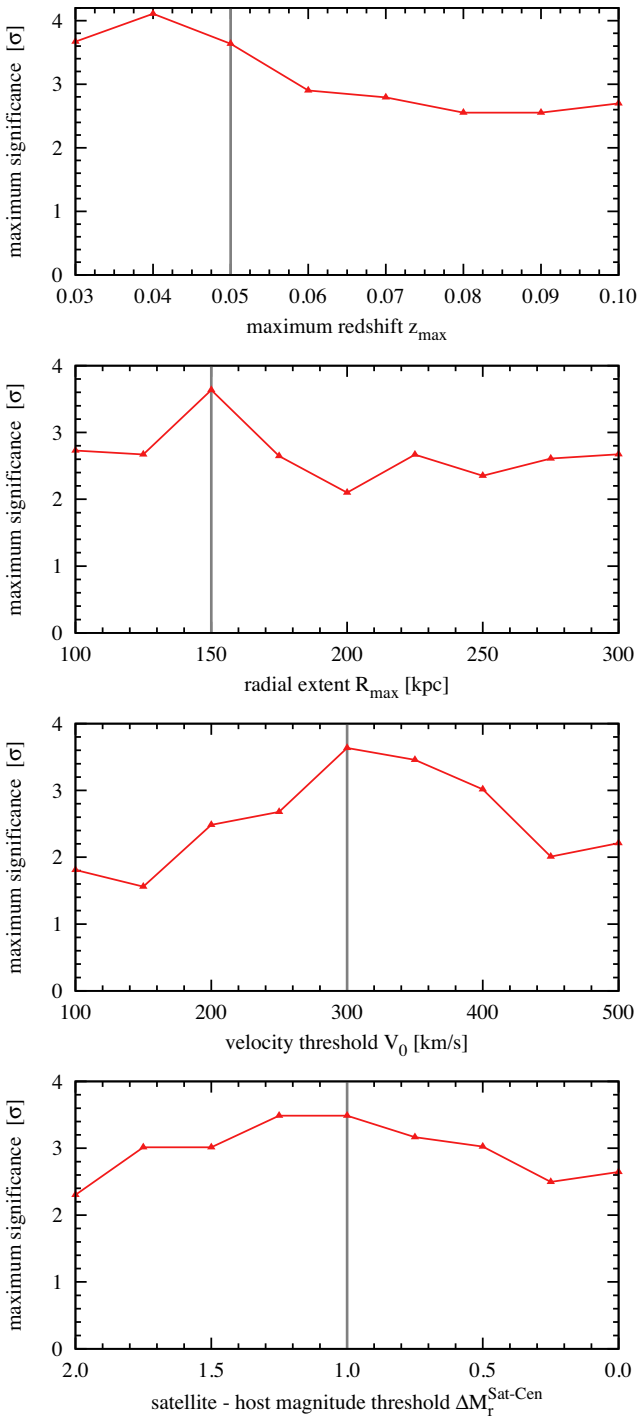

Figure 7. The maximum significance of the excess of satellite pairs with anticorrelated velocities over the tolerance angle range $5^\circ \leq \alpha \leq 30^\circ$, as a function of different sample selection criteria. For all cases, we retain the same selection parameters as in the reference case of Ibata14 but vary, in turn, the maximum redshift (top panel), the radial extent of the volume over which satellites are found (second panel), the maximum velocity difference with respect to the primary (third panel), and the magnitude difference between primary and satellite (bottom panel). The grey lines indicate the choices made in the reference model of Ibata14. In each panel, the sample size increases from left to right.

Table 2. The fraction of diametrically opposed pairs with anticorrelated velocity and the significance of the excess when varying the sample selection criteria. We give the results for a tolerance angle, $\alpha = 8^\circ$, that corresponds to the maximum significance shown in Fig. 7. The column in grey corresponds to the reference selection criteria of Ibata14.

$z_{\rm max}$ variation	$z_{\rm max}$ values	0.03	0.04	0.05	0.06	0.07	0.08	0.10
	Anticorrelated/total pairs	10/10	18/19	20/23	21/27	22/29	22/30	23/31
	Significance [σ]	3.7	4.1	3.6	2.9	2.8	2.6	2.7
$R_{\rm max}$ variation	$R_{\rm max}$ values	100	125	150	175	200[a]	250[a]	300[a]
	Anticorrelated/total pairs	10/11	14/17	20/23	21/28	24/37	38/65	48/80
	Significance [σ]	2.7	2.7	3.6	2.6	1.8	1.3	1.8
$V_{\rm max}$ variation	$V_{\rm max}$ values	200	250	300	350	400	450	500
	Anticorrelated/total pairs	11/13	12/14	20/23	23/28	27/36	31/48	34/52
	Significance [σ]	2.5	2.7	3.6	3.5	3.0	2.0	2.2
$\Delta M_r^{\rm Sat-Cen}$ variation	$\Delta M_r^{\rm Sat-Cen}$ values	1.50	1.25	1.00	0.75	0.50	0.25	0.00
	Anticorrelated/total pairs	17/20	20/23	20/23	20/24	21/26	21/28	22/29
	Significance [σ]	3.2	3.6	3.6	3.3	3.2	2.6	2.8

Note. [a]The $R_{\rm max} = 200$, 250 and 300 kpc entries have the maximum excess of anticorrelated pairs for $\alpha = 6^\circ$, for which there are 19/27, 26/36 and 31/46 anticorrelated pairs that correspond to a 2.1, 2.4 and 2.7σ excess. At $\alpha = 6^\circ$, the reference sample has 15/17 anticorrelated pairs.

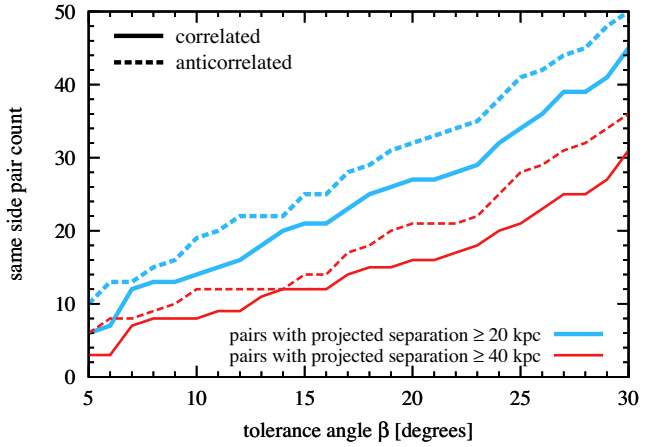

Figure 8. The number of same side satellite pairs with correlated and anticorrelated velocities as a function of the tolerance angle, β. We present results for satellite pairs separated in projected distance by more than 20 kpc (thick lines) and more than 40 kpc (thin lines).

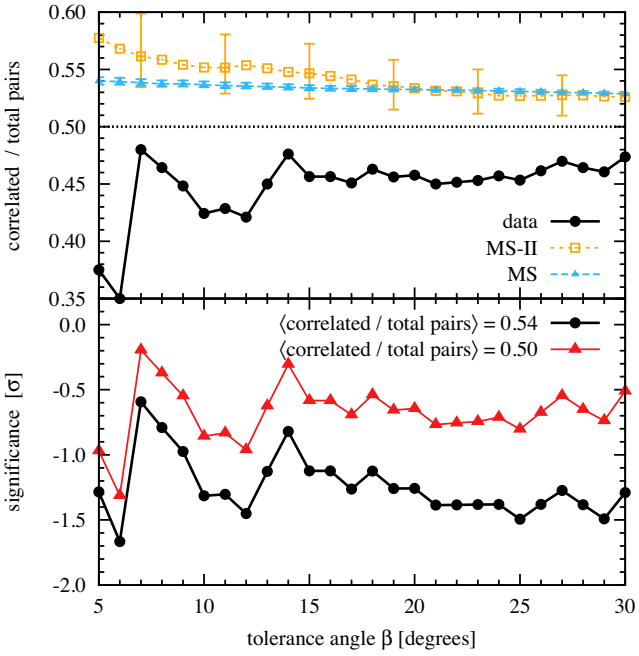

Figure 9. Top panel: the excess of satellite pairs with correlated velocities as a function of the tolerance angle, β, for pairs found on the same side of the primary. We compare the observational data (solid black) with results from the MS (blue crosses) and MS-II (orange open squares). The signature of rotating discs of satellites is an excess of pairs with correlated velocities. In contrast, the data show a small deficit of pairs with correlated velocities. The error bars for the MS and MS-II data show 1σ bootstrap uncertainties. Bottom panel: the significance of the excess of satellite pairs with correlated velocities compared to the MS predictions (circles; mean expectation of 0.54) and to a uniform distribution (triangles; mean expectation of 0.5). The negative values for the significance reflect the fact that instead of an excess, we find a deficit of correlated pairs.

but opposite excess of *correlated* velocities would be expected for pairs of satellites on the same side of the primary. This provides an independent test of the significance of the result reported in the previous section. For same-side satellite pairs, we use the same selection criteria as described in Section 2 and in Ibata14, but also require the projected distance between satellites to be greater than 20 kpc. In the SDSS sample, due to fibre collisions, very few satellite pairs are closer than this separation, so we require projected separations ≥ 20 kpc in order to make sure that the mocks do not include close pairs likely to be absent in the real data.

The number of same side pairs with correlated and anticorrelated velocities is shown in Fig. 8. We find no significant difference in the number of pairs with correlated and anticorrelated velocities, within the expected scatter of a binomial distribution. The same result holds if we increase the minimum separation between pairs to 40 kpc, although in this case the sample is, of course, smaller. For the remainder of this section, we consider pairs with a projected separation ≥ 20 kpc, to make use of the better statistics available for his sample. The number of same-side pairs at the tolerance angle, $\beta = 8^\circ$, is 28, which is only slightly larger than the total count of 23 diametrically opposed pairs. Therefore, same-side pairs have similar or better statistical power to test for the presence of rotating discs of satellite galaxies.

Fig. 9 shows the fractional abundance of correlated velocities and its significance as a function of the tolerance angle, β, for same-side satellite pairs. Instead of the expected excess, we find a small deficit of pairs with correlated velocities, although the result is consistent,

within 1σ, with a uniform distribution and only marginally inconsistent, $\sim 1.5\sigma$, with the results from the mock catalogue. Even in the absence of discs, the MS and MS-II simulations predict a slight excess, 54 per cent, of correlated velocity pairs, which may be due to binary satellites orbiting around the brighter primary.[4] The idea of rotating discs of satellites is disfavoured by the lack of excess of same-side pairs with correlated velocities and supports the low significance of the excess of anticorrelated velocities for opposite-side pairs found in the preceding section.

5 CONCERNS RAISED BY IBATA ET AL.

A few weeks after submitting our paper to the arXiv, Ibata et al. (2014b, hereafter Ibata14-b) posted a paper in which they included a response to the concerns we had expressed in our original submission about Ibata14's earlier results. In the remainder of this section, we address their response and show that our initial critique of the robustness of the detection of a rotating disc of satellites remains valid.

5.1 Spatial distribution

Ibata14-b investigated the spatial anisotropy of satellites by counting, as a function of opening angle, all satellite pairs in which one member is a spectroscopically-confirmed satellite of the primary, while the second is a photometric-redshift satellite candidate. This is very similar to the analysis we presented in Section 3, with the difference that Ibata14-b considers all the spectroscopically-confirmed satellites of a primary, not only the brightest one as in our case. In practice, this difference is unimportant since most primaries have only one such satellite. Thus, their fig. 3 is equivalent to the $90^\circ \leq \theta_{\rm BS\cdot S} \leq 180^\circ$ region of our Figs 1–3, where their angle definition is the complement of our angle, $\theta_{\rm BS\cdot S}$.

Due to limited statistics, Ibata14-b focused their analysis on the ratio, $N_{\rm O}/N_{\rm A}$, between the number of satellites with $135^\circ \leq \theta_{\rm BS\cdot S}$ and the number with $90^\circ \leq \theta_{\rm BS\cdot S} \leq 135^\circ$, finding a ratio of $\sim$3. This is in stark contrast to our analysis which finds a significantly lower value of $N_{\rm O}/N_{\rm A} = 1.1$. In fact, a value of 3 is unphysical as may be easily verified using simplified models such as the one we introduced in Section 3.1. We generated mock catalogues from such simplified models, to which we applied the same primary and satellite selection criteria as Ibata14-b. The case when 50 per cent of satellites are on a thin plane, with the rest distributed isotropically, gives $N_{\rm O}/N_{\rm A} = 1.1$. Even in the most extreme case, when all the satellites are on an infinitely thin plane, the $N_{\rm O}/N_{\rm A}$ ratio cannot be higher than $\sim$1.4. This is because the $N_{\rm O}/N_{\rm A}$ ratio measures the anisotropies of the satellite distribution as projected on the plane of the sky. The anisotropy is largest for satellite planes seen edge-on, and decreases rapidly to zero as the viewing angle approaches a face-on planar configuration. The signal is further diminished by contamination from interloper galaxies that have a small line-of-sight velocity difference with respect to the primary and thus are mistaken as spectroscopically confirmed satellites (see Fig. 1 for a qualitative estimate of this effect).

We suspect that the high $N_{\rm O}/N_{\rm A}$ ratio found by Ibata14-b is due to an overestimation of the background contamination. Even a small change in the background count will result in a large change in the $N_{\rm O}/N_{\rm A}$ value. For example, a decrease in the background fraction from their quoted value of 85 per cent to a more modest 80 per cent would lower the Ibata14-b result to $N_{\rm O}/N_{\rm A} = 2.1$. A similar, or even larger, decrease in background fraction is not unlikely given that Ibata14-b used a new background estimation method that has not been tested in any systematic way. Their background contamination was estimated using bright satellites (apparent magnitude $r \lesssim 17.7$) with spectroscopic redshifts and then extrapolating the result to much fainter objects ($r \lesssim 19.5$). In contrast, our background contamination is estimated in a very robust way using a method that has been thoroughly and independently tested and applied by several groups (among others by Nierenberg et al. 2012; Guo et al. 2012; WW12).

Secondly, Ibata14-b's choice of radial extent used to identify satellites, between 100 and 150 kpc, was motivated by the presence of a peak at these radii seen in their Fig. 5. Given that for radial distances $\lesssim$180 kpc all the data points agree well within the 1σ uncertainty, the peak is more likely to be a statistical fluctuation rather than a real signal. Such a posteriori choice of the radial extent that maximizes the enhancement will inevitably lead to an excess in the $N_{\rm O}/N_{\rm A}$ ratio due solely to statistical fluctuations.

5.2 Diametrically opposed pairs

Ibata14-b put forward several reasons attempting to explain why we find a decrease in the excess of anticorrelated pairs in their diametrically opposed-pair test when we vary their sample selection criteria. They used these arguments to downplay the results of Section 4.1 above but, unfortunately, they did not check if their arguments are actually valid in practice. For simplicity, we address their concerns regarding the variation of the $R_{\rm max}$ and $V_{\rm max}$ selection parameters since, when relaxing these, we obtain the largest number of new satellite pairs (see Table 2 and the discussion in Section 4.1). Thus, relaxing these selection criteria offers the cleanest way to assess the robustness of the results presented in Ibata14.

Ibata14-b stated that increasing the maximum radial extent, $R_{\rm max}$, or the maximum line-of-sight velocity difference, $V_{\rm max}$, leads to a significant increase in contamination by interloper galaxies that are not true satellites of the primary. This appears very unlikely, since, as can be seen in Fig. 10, most of the primaries found in the original sample of Ibata14 are very bright, with virial radii significantly larger than 150 kpc and with satellite velocity dispersions larger than Andromeda's. Increasing $R_{\rm max}$ or $V_{\rm max}$ does not introduce any bias in the primaries around which satellites are found: a Kolmogorov–Smirnov test indicates that all five distributions of primary magnitudes shown in Fig. 10 are consistent with one another at 99 per cent confidence. Thus, by increasing $R_{\rm max}$ or $V_{\rm max}$ we simply find more satellite pairs around primaries similar to the ones in the reference sample.

We can estimate the contamination fraction due to interloper galaxies using our MS-II mock catalogues which have a similar background to the real data. For this, we find the fraction of MS-II satellite pairs in which one or both members of the pair are not part of the same FOF halo as the isolated primary. This interloper fraction is highly dependent on the brightness of the primary, so we compute it for each of the six primary magnitude bins shown in Fig. 10. For example, the contamination fraction for satellite pairs selected using the reference criteria around centrals with $-20.5 \leq M_{\rm r}^{\rm Cen} \leq -20.0$ is 18 per cent and this fraction decreases to 3.5 per cent for centrals with $-23.0 \leq M_{\rm r}^{\rm Cen} \leq -22.5$. To find the mean contamination for each sample, we weigh the contamination fraction found for each primary magnitude bin by the number of primaries in that bin.

[4] For diametrically opposed pairs the simulations predict a approximatively equal numbers of anticorrelated and correlated velocity pairs.

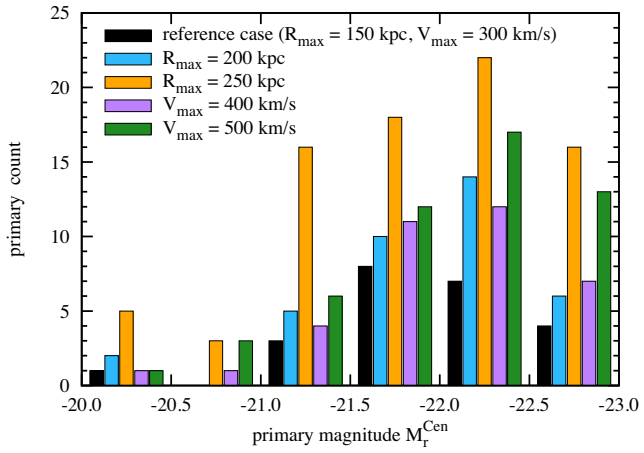

Figure 10. The histogram of absolute *r*-band magnitudes, $M_{\rm r}^{\rm Cen}$, for isolated primaries that host a diametrically opposed satellite pair within a tolerance angle, $\alpha = 8^{\circ}$. Results are presented for several sample selection criteria: the reference sample as in Ibata14; when increasing the maximum projected radial extent from $R_{\rm max} = 150$ to 200 and 250 kpc; and when increasing the maximum velocity difference with respect to the primary from $V_{\rm max} = 300$ to 400 and 500 km s^{-1}.

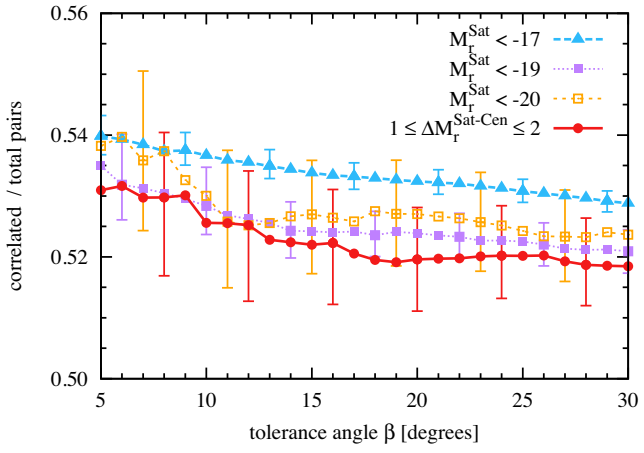

Figure 11. The excess of same-side satellite pairs with correlated velocities predicted in the MS simulation mock catalogue for satellites of different luminosity. The excess is largely independent of satellite luminosity and even very bright satellite pairs, within 1 to 2 mag from their primaries, show a similar signal. Thus, the lack of a signature of rotating satellite systems in the same-side pair test cannot be due to the presence of bright binary pairs. The solid triangles correspond to then blue crosses in the top panel of Fig. 9. Note the very different scales used in the two figures.

For the reference sample, we find a mean contamination fraction of 6 per cent. When we increase $V_{\rm max}$ from 300 to 400 and 500 km s^{-1} we find the same mean contamination fraction of 6 per cent. The reason for this is that while the contamination fraction for each primary magnitude bin increases, the fraction of brighter primaries is slightly higher than in the reference case, so that, on average, the mean sample contamination hardly changes. When we increase $R_{\rm max}$ from 150 to 200, 250 and 300 kpc, we find a slight increase in contamination from 6 to 8, 10 and 12 per cent, respectively. Thus, the change in mean sample contamination is minor and cannot possibly explain why satellite pairs found at $V_{\rm max} > 300$ km s^{-1} or $R_{\rm max} > 150$ kpc do not show any excess of anticorrelated over correlated velocities (see discussion in Section 4.1).

5.3 Same side pairs

In Fig. 11, we investigate if the lack of a rotating disc signal for same-side pairs is due to the inclusion of close and bright binary satellite pairs, as suggested by Ibata14-b. The ΛCDM data show that the same excess of correlated pairs independently of the brightness of the pair members. The excess is roughly the same even when considering only pairs in which both members have a magnitude difference with respect to the primary, $\Delta M_{\rm r}^{\rm Sat-Cen}$, in the range $1 \leq \Delta M_{\rm r}^{\rm Sat-Cen} \leq 2$. Thus, contrary to the assertion by Ibata14-b, close and bright binary satellites do not reduce the signature of a rotating disc of satellites. Discarding pairs in which one member has $\Delta M_{\rm r}^{\rm Sat-Cen} \leq 2$, as suggested by Ibata14-b, serves only to lower the statistics without gaining any useful information.

In conclusion, we find that the proposals of Ibata14-b cannot explain why the significance of the result obtained by Ibata14 decreases when varying the sample selection criteria. In particular, we have explicitly shown that the absence of an excess of anticorrelated over correlated velocity pairs for $V_{\rm max} > 300$ km s^{-1} and $R_{\rm max} > 150$ kpc cannot be due to an increase in the contamination rate by interloper galaxies, as claimed by Ibata14-b. Similarly, we have shown that the absence of a rotating disc signature for same-side pairs cannot be due to close and bright binary satellites since such pairs, in fact, enhance, not reduce, the signature of rotating satellite systems. Furthermore, we find that the high spatial anisotropy in the spatial distribution of satellites reported by Ibata14-b exceeds the expectation of the most extreme case, when all satellites are distributed in an infinitely thin plane. This unphysical result is most likely due to an overestimation of the background contamination fraction.

6 DISCUSSION AND CONCLUSIONS

In the first part of this study, we characterized the spatial distribution of satellites in a large sample of SDSS galaxies. Our analysis focused on isolated primaries that have one or more satellites with spectroscopic redshifts. We used the photometric catalogue of SDSS/DR8 galaxies to count the number of satellites as a function of the angle they subtend relative to a reference axis defined by the brightest satellite. We considered three samples of primary galaxies centred on absolute magnitudes of $M_{\rm r} = -23$, -22 and -21. We found a clear signal of anisotropy in the spatial distributions of satellites of the two brightest samples of primaries, while for the faintest sample the uncertainties are of the same order as the expected signal. We compared the observational data to the predictions of the semi-analytic galaxy formation model of Guo et al. (2011) implemented in the ΛCDM Millennium and Millennium-II cosmological simulations, and find very good agreement between the observations and the theoretical predictions.

In the second part of this study, we extended the analysis of Ibata14 to explore if the anisotropy we detected could be related to the rotating discs of satellites claimed by these authors. We concluded that the observational sample is not robust enough to detect such discs. However, we stress that rotating satellite systems do exist in ΛCDM (Lovell et al. 2011) but not to the extent reported by Ibata14. In particular, we found the excess of diametrically opposed pairs with anticorrelated velocities seen by Ibata14 to be very sensitive to the sample selection criteria. Small variations from the reference criteria employed by these authors lead to smaller

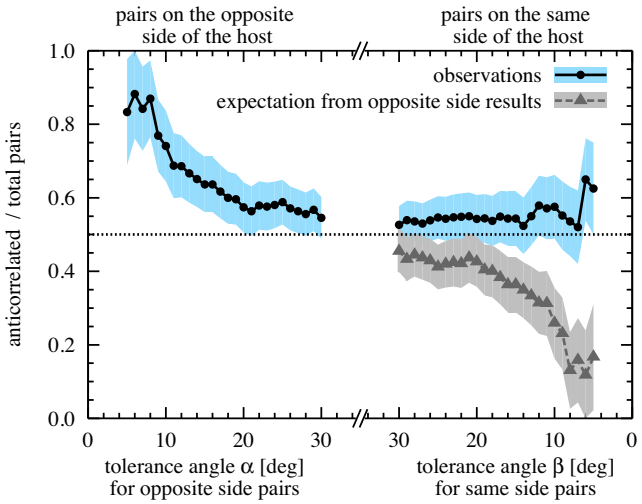

Figure 12. Comparison of the excess of satellite pairs with anticorrelated velocities for pairs diametrically opposite (left-half) and on the same side (right-half) of the primary. The observational results are shown by the filled circles. The filled triangles show the expected signal if the results found for diametrically opposite pairs were indicative of a rotating disc of satellites (it is a mirror image of the left-half results with respect to the $y = x$ diagonal). The shaded region shows the 1σ uncertainty.

excesses of anticorrelated pairs and, almost invariably, to a reduced significance, which in many cases is well below 3σ.

In general, when the selection criteria applied by Ibata14 are relaxed, for example by extending the radial acceptance range, the additional pairs found show no signal of rotation at all. Thus, increasing the maximum radial extent, $R_{\rm max}$, from the reference value of 150 to 300 kpc adds 57 new satellite pairs (compared to 23 in the reference sample), of which 28 have anticorrelated velocities and 29 have correlated velocities. Similarly, increasing the maximum line-of-sight velocity difference relative to the host, $V_{\rm max}$, from the reference value of 300 to 500 km s^{-1} adds 29 pairs, of which 14 have anticorrelated velocities and 15 correlated velocities.

Thus, the reason why perturbed samples still appear to show a significant signal, albeit not as significant as the reference sample, is simply that all these samples are all correlated and include most, if not all, of the 23 pairs in the reference sample responsible for the original excess of anticorrelated over correlated pairs. The absence of any signal outside the reference sample cannot be attributed to interloper contamination, as we showed in Section 5. The sensitivity of the rotation signal to the sample selection criteria leads us to conclude that the claimed detection of rotating satellite discs in the SDSS data is not robust.

To test further if the reported excess of anticorrelated velocities among satellites on opposite sides of the primary could originate from a large fraction of systems having rotating discs of satellites, we compared it to the expected excess of correlated velocities among satellites on the same side of their respective primaries. Using similar selection criteria to those used by Ibata14 to define the opposite side pairs, we found no excess of correlated velocities in same side pairs in the SDSS sample. The absence of such an excess cannot be attributed to confusion introduced by the inclusion of bright binary satellites, as we showed in Section 5.

The results for opposite and same side satellite systems are summarized in Fig. 12, which shows the fraction of anticorrelated pairs of satellites on either the opposite or the same side of their host primary. Filled circles show the actual measurements on both sides, while on the right half, grey triangles denote the expected signal for same side pairs if the excess of anticorrelated velocities measured for diametrically opposed pairs were indicative of rotating discs. The measurements for same side pairs are clearly in disagreement with this hypothesis, especially at small tolerance angle, β, where the signal of a rotating disc is expected to be maximal. This lack of any rotation signal among same side satellites and the discrepancy with the reported signal from opposite side satellites further weakens the evidence for universally rotating satellite systems.

While exposing the lack of robustness of the detection claimed by Ibata14, our analysis cannot exclude the possibility that the $\sim 3.5\sigma$ excess of anticorrelated overcorrelated pairs that they found is indeed a signature of rotating satellite systems. Such systems would have to have a projected radial extent of 150 kpc and a maximum line-of-sight velocity difference relative to the host of 300 km s^{-1}, since the signal is much reduced when either of these parameters is varied. We find this possibility rather unlikely. The choice of these parameters by Ibata14 was motivated by reference to earlier work on the PAnDAS survey of M31 whose footprint extends to 150 kpc, while the velocity threshold, $V_{\rm max} = 300$ km s^{-1}, corresponds to twice the central velocity dispersion of M31. Not only are these choices arbitrary, but their relevance is unclear given that the primaries in the sample of Ibata14 are all much brighter than M31. We are led to conclude that detection by Ibata14 represents an $\sim 3.5\sigma$ statistical fluctuation, a conclusion that is further strengthen by the complete absence of a signal for same-side pairs even in their own sample.

It might be argued that perhaps satellite planes have an intrinsic scale determined by an as yet unknown physical process. In this case, it could be further argued that relaxing the Ibata14 sample selection criteria would weaken the signal of the rotating satellite plane. Such a hypothesis, however, is problematic. It is inconsistent with the lack of any rotation signal in the same-side pairs test. In addition, it also appears inconsistent with the results of varying $V_{\rm max}$ in the diametrically-opposed pairs test. As we saw, the significance of the detection of rotation decreases rapidly with increasing $V_{\rm max}$. Yet, at least in the MS-II mocks (which reproduce the radial satellite distribution of SDSS centrals reasonably well - see Wang et al. 2014), the 3D radial distribution of satellites within a fixed projected radius varies only slightly when increasing $V_{\rm max}$. For example, within a projected distance of 150 kpc and for $V_{\rm max} = 300$ km s^{-1}, corresponding to Ibata14's sample, on average only 49 per cent of pairs have both members within a 3D radial distance of 150 kpc. By increasing $V_{\rm max}$ to 400 and 500 km s^{-1}, the number of pairs within this 3D radial distance decreases slightly to 47 per cent and 45 per cent, respectively. Thus, the different $V_{\rm max}$ cuts we have considered do not significantly affect the radial extent of the sample. Yet, the additional pairs added to the sample when increasing $V_{\rm max}$ from 300 to 500 km s^{-1} show no signal of rotation.

The spatial and kinematic distributions of the satellites around the MW and, more recently, around Andromeda have been deemed a serious challenge to the ΛCDM model by several recent authors (e.g. Kroupa, Theis & Boily 2005; Pawlowski et al. 2012a; Ibata et al. 2013) on the grounds that ΛCDM haloes seldom have satellite distributions that are as flattened and showing the same degree of coherent rotation as found in the LG (Wang et al. 2013; Bahl & Baumgardt 2014; Ibata et al. 2014c). Our own analysis of the spatial and kinematic distributions of the satellites around a large sample of SDSS galaxies, returns results that are generally in very good agreement with ΛCDM predictions. The satellite systems are indeed flattened and exhibit a moderate degree of coherent rotation. According to ΛCDM simulations, these properties reflect the

accretion of satellites along filaments of the cosmic web. Further characterization of satellites systems and of the cosmic web, together with increasingly realistic cosmological simulations, should reveal the nature of this connection in greater detail.

ACKNOWLEDGEMENTS

We are grateful to Rodrigo Ibata for useful and helpful discussions; and to Shaun Cole, Wojtek Hellwing and Qi Guo for discussions during the early stages of the project. We thank the anonymous referee for a careful reading of our paper and for detailed comments that have helped us improve it. This work was supported in part by ERC Advanced Investigator grant COSMIWAY [grant number GA 267291] and the Science and Technology Facilities Council [grant number ST/F001166/1, ST/I00162X/1]. WW is supported by JRF grant number RF040353. This work used the DiRAC Data Centric system at Durham University, operated by ICC on behalf of the STFC DiRAC HPC Facility (www.dirac.ac.uk). This equipment was funded by BIS National E-infrastructure capital grant ST/K00042X/1, STFC capital grant ST/H008519/1 and STFC DiRAC Operations grant ST/K003267/1 and Durham University. DiRAC is part of the National E-Infrastructure. This research was carried out with the support of the 'HPC Infrastructure for Grand Challenges of Science and Engineering' Project, co-financed by the European Regional Development Fund under the Innovative Economy Operational Programme.

REFERENCES

Abazajian K. N. et al., 2009, ApJS, 182, 543
Agustsson I., Brainerd T. G., 2010, ApJ, 709, 1321
Aihara H. et al., 2011, ApJS, 193, 29
Bahl H., Baumgardt H., 2014, MNRAS, 438, 2916
Bailin J., Power C., Norberg P., Zaritsky D., Gibson B. K., 2008, MNRAS, 390, 1133
Blanton M. R. et al., 2005, AJ, 129, 2562
Boylan-Kolchin M., Springel V., White S. D. M., Jenkins A., Lemson G., 2009, MNRAS, 398, 1150
Brainerd T. G., 2005, ApJ, 628, L101
Crain R. A. et al., 2009, MNRAS, 399, 1773
Cunha C. E., Lima M., Oyaizu H., Frieman J., Lin H., 2009, MNRAS, 396, 2379
Deason A. J. et al., 2011, MNRAS, 415, 2607
Forero-Romero J. E., Hoffman Y., Yepes G., Gottlöber S., Piontek R., Klypin A., Steinmetz M., 2011, MNRAS, 417, 1434
Fouquet S., Hammer F., Yang Y., Puech M., Flores H., 2012, MNRAS, 427, 1769
Guo Q. et al., 2011, MNRAS, 413, 101
Guo Q., Cole S., Eke V., Frenk C., 2012, MNRAS, 427, 428
Hammer F., Yang Y., Fouquet S., Pawlowski M. S., Kroupa P., Puech M., Flores H., Wang J., 2013, MNRAS, 431, 3543
Ibata R. A. et al., 2013, Nature, 493, 62
Ibata N. G., Ibata R. A., Famaey B., Lewis G. F., 2014a, Nature, 511, 563 (Ibata14)
Ibata R. A., Famaey B., Lewis G. F., Ibata N. G., Martin N., 2014b, preprint (arXiv:1411.3718) (Ibata14-b)
Ibata R. A., Ibata N. G., Lewis G. F., Martin N. F., Conn A., Elahi P., Arias V., Fernando N., 2014c, ApJ, 784, L6
Koch A., Grebel E. K., 2006, AJ, 131, 1405
Kroupa P., 2012, PASA, 29, 395
Kroupa P., Theis C., Boily C. M., 2005, A&A, 431, 517
Lares M., Lambas D. G., Domínguez M. J., 2011, AJ, 142, 13
Libeskind N. I., Frenk C. S., Cole S., Helly J. C., Jenkins A., Navarro J. F., Power C., 2005, MNRAS, 363, 146
Libeskind N. I., Frenk C. S., Cole S., Jenkins A., Helly J. C., 2009, MNRAS, 399, 550
Libeskind N. I., Knebe A., Hoffman Y., Gottlöber S., Yepes G., Steinmetz M., 2011, MNRAS, 411, 1525
Libeskind N. I., Knebe A., Hoffman Y., Gottlöber S., 2014, MNRAS, 443, 1274
Li Y.-S., Helmi A., 2008, MNRAS, 385, 1365
Lovell M. R., Eke V. R., Frenk C. S., Jenkins A., 2011, MNRAS, 413, 3013
Lynden-Bell D., 1976, MNRAS, 174, 695
McConnachie A. W., Irwin M. J., 2006, MNRAS, 365, 902
McConnachie A. W. et al., 2009, Nature, 461, 66
Metz M., Kroupa P., Libeskind N. I., 2008, ApJ, 680, 287
Metz M., Kroupa P., Jerjen H., 2009a, MNRAS, 394, 2223
Metz M., Kroupa P., Theis C., Hensler G., Jerjen H., 2009b, ApJ, 697, 269
Nierenberg A. M., Auger M. W., Treu T., Marshall P. J., Fassnacht C. D., Busha M. T., 2012, ApJ, 752, 99
Pawlowski M. S., Kroupa P., 2013, MNRAS, 435, 2116
Pawlowski M. S., McGaugh S. S., 2014, ApJ, 789, L24
Pawlowski M. S., Pflamm-Altenburg J., Kroupa P., 2012a, MNRAS, 423, 1109
Pawlowski M. S., Kroupa P., Angus G., de Boer K. S., Famaey B., Hensler G., 2012b, MNRAS, 424, 80
Pawlowski M. S. et al., 2014, MNRAS, 442, 2362
Shaw L. D., Weller J., Ostriker J. P., Bode P., 2006, ApJ, 646, 815
Springel V. et al., 2005, Nature, 435, 629
Springel V. et al., 2008, MNRAS, 391, 1685
Wang W., White S. D. M., 2012, MNRAS, 424, 2574 (WW12)
Wang J., Frenk C. S., Cooper A. P., 2013, MNRAS, 429, 1502
Wang W., Sales L. V., Henriques B. M. B., White S. D. M., 2014, MNRAS, 442, 1363
Warnick K., Knebe A., 2006, MNRAS, 369, 1253
Yang X., van den Bosch F. C., Mo H. J., Mao S., Kang X., Weinmann S. M., Guo Y., Jing Y. P., 2006, MNRAS, 369, 1293
Yang Y., Hammer F., Fouquet S., Flores H., Puech M., Pawlowski M. S., Kroupa P., 2014, MNRAS, 442, 2419
Zentner A. R., Kravtsov A. V., Gnedin O. Y., Klypin A. A., 2005, ApJ, 629, 219

This paper has been typeset from a TEX/LATEX file prepared by the author.